

Ferroelectric Thickness Dependent Domain Interactions in FEFETs for Memory and Logic: A Phase-field Model based Analysis

A. K. Saha¹, M. Si¹, K. Ni², S. Datta³, P. D. Ye¹, and S. K. Gupta¹

¹Purdue University, ²Rochester Institute of Technology, ³University of Notre Dame, email: saha26@purdue.edu

Abstract— We present a phase-field simulation framework for ferroelectric (FE)-FET which captures multi-domain effects by self-consistently solving 2D time-dependent Ginzburg-Landau (TDGL), Poisson's, and semiconductor charge/transport equations. Using our phase-field model and experiments, we analyze electrostatics-driven multi-domain formation and voltage-induced polarization (P) switching for different FE thickness (T_{FE}). We show that for $T_{FE} = 5\text{nm} - 10\text{nm}$, FEFETs exhibit multi-level memory functionality; while for $T_{FE} = 1.5\text{nm} - 3\text{nm}$, FEFETs can serve as non-hysteretic switches with enhanced gate control. Our results signify that as T_{FE} is reduced from 10nm to 5nm, denser domain patterns emerge in FE, and the dominant P -switching mechanism changes from nucleation to domain-wall motion based leading to a decreased memory window with T_{FE} scaling. Moreover, as T_{FE} is scaled further from 3nm to 1.5nm, effective permittivity of the gate stack increases due to multi-domain electrostatic interactions.

I. INTRODUCTION

By virtue of its CMOS process compatibility, Hafnium Zirconium Oxide (HZO) based FEFET is emerging as one of the most promising candidates for future electronics. FEFET have been demonstrated to offer multi-level memory/synaptic functionalities for high FE thickness (T_{FE} -10nm) [1-2] (Fig. 1(b)) and non-hysteretic switch behavior with enhanced gate control for low T_{FE} (<3nm) (Fig.1(c)) [3-4]. However, the multi-domain effects in FE and its correlation with T_{FE} , as well as the enhanced permittivity (ϵ_r) behavior is yet to be understood. To that end, in this work, we analyze multi-domain polarization (P) switching and the origin of enhanced- ϵ_r in FEFETs and their dependence on T_{FE} . Our analysis is based on self-consistent phase-field model of FEFET, validated with our experimental characteristics of metal-ferroelectric-insulator-metal (MFIM) and metal-ferroelectric-insulator-semiconductor (MFIS) stack for different T_{FE} . Unlike previous FEFET models [5-8], which assume a certain number of FE domains [5], in our model, the multi-domain formation in the FE is self-consistently determined by electrostatics, which allows us to comprehensively analyze the microscopic domain interactions in FE and its influence on the underlying transistor channel. Using our model, we provide several insights into the T_{FE} -dependent behavior of FEFETs.

II. PHASE-FIELD MODELING OF FEFET

In our phase-field simulation, we self-consistently solve the TDGL equation [9-10] for P , Poisson's equation for potential and semiconductor charge equations for charge density profile. The considered FEFET structure, simulation flow and parameters are shown in Fig. 3. We consider HZO ($\text{Hf}_{0.5}\text{Zr}_{0.5}\text{O}_2$) as FE, where the P direction is assumed to be along the film thickness, which is analogous to the c -axis of its orthorhombic crystal phase. In addition, the Landau coefficients used in simulation are assumed to be strain normalized based on the assumption of a stress free

interface. Note, unlike a previous FEFET model [6] based on 1D Landau-Khalatnikov equation, we use 2D TDGL equation to capture P variation along the FE thickness. Other advancements of our model are summarized in Fig. 2.

III. VALIDATION OF PHASE-FIELD MODEL

To validate our phase-field model, we fabricate and measure the P - V characteristics of MFIM (HZO- Al_2O_3) stack. Our simulation results (Fig. 4(a-c)) signify good agreements with the measured P - V characteristics for different T_{FE} (5, 7 and 10nm). The P profile of the FE at 0V in Fig. 4(d) suggests the formation of multi-domain (MD) state. Formation of such MD state occurs to suppress the depolarization electric(E)-field in FE by forming in-plane E -field (stray field) in the FE-DE interface (Fig. 5). In addition to the electrostatic energy associated with stray field, there is a gradient energy ($\sim(dP/dx)^2$) associated with the P variation near the domain-wall (DW). With the decrease in T_{FE} , the span of DW (along the z -axis) decreases, which reduces the gradient energy of DW. This leads to the formation of larger number of domains with decreasing T_{FE} (Fig. 4(d)), which suppresses the depolarization E -field in FE more effectively. As the number of domains in the FE layer depends on electrostatic interaction between the FE and DE layer, the DE layer thickness (T_{DE}) as well as its permittivity impacts the number of domains. The simulated and measured major/minor P - V characteristics of 10nm HZO with T_{DE} =3nm and 5nm are shown in Fig. 6(a) and Fig. 7(a), respectively, showing good agreement. For T_{DE} =3nm, the domain pattern is less dense compared to T_{DE} =5nm. Therefore, the depolarization-field is more significant in the former case. As a result, the applied voltage driven P -switching in FE for T_{DE} =3nm takes place as a combination of domain nucleation and DW motion (Fig. 6(b)). However, for T_{DE} =5nm, the domain pattern is relatively denser and hence, the P -switching takes place only through DW motion (Fig. 7(b)). The number of domains for different T_{FE} are shown in Fig. 8 suggesting denser domains with decreasing T_{FE} . Therefore, T_{FE} scaling should prefer DW motion-based P -switching over domain nucleation. Based on this understanding, let us now discuss the FEFET characteristics and their dependence on T_{FE} scaling.

IV. MULTI-LEVEL MEMORY FUNCTIONALITY

We first analyze the FEFETs for T_{FE} scaled from 10nm to 5nm. The simulated gate charge (Q) versus gate voltage (V_{GS}) for T_{FE} =10nm (Fig. 9) shows hysteretic characteristics with a two-step increase (decrease) in Q during the forward (reverse) sweep. The P profile of FE layer (Fig. 10) suggests that, with the increase in V_{GS} , P -switching first happens through nucleation of new + P domain at the source (S) and drain (D) side of FE giving rise to a sharp increase in Q - V_{GS} characteristics. With the further increase in V_{GS} , the - P domain between the newly nucleated + P and the previous + P domains completely switches to + P through DW motion. This gives rise to second step in the Q - V_{GS} characteristics. Note that the reason for dominant P -switching at the S/D side is the higher E -

field (originating from the depletion regions in S/D) compared to the center of the FE. Considering the SET and RESET condition (after applying $V_G=+5V$ and $V_G=-5V$, respectively), the potential profile of the FEFET is shown in Fig. 11 for $V_G=0V$, illustrating highly non-uniform potential distribution in the channel due to MD state of FE. For RESET state, domains near the S/D side are in $-P$ state which induce a large negative potential across the channel-S/D junction. In contrast, for SET state, due to the dominant $+P$ domain near the S/D side, the potential across the channel-S/D junction becomes positive. As a result of P -induced change in channel potential, we observe a large V_T ($=V_{GS}$ at $I_D=1\mu A/\mu m$) shift in the I_D - V_{GS} characteristics of FEFET between RESET and SET states (Fig. 12). Moreover, due to the step wise P -switching in the FE layer, different V_T shift in the I_D - V_{GS} characteristics of FEFET are obtained for different V_{SET} value as shown in Fig. 12, leading to multi-level memory behavior.

Similar to $T_{FE}=10nm$, Q - V_G characteristics for $T_{FE}=5nm$ (Fig. 13) signifies hysteretic characteristics with smaller step-wise change in Q . This is because for lower T_{FE} (5nm), the domain density is more (compared to $T_{FE}=10nm$). Hence, V_G -induced P -switching takes place via DW motion (Fig. 14) leading to a smaller step-wise change in Q - V_G characteristics. Similar to $T_{FE}=10nm$, the P -switching for $T_{FE}=5nm$ is more dominant near S/D (Fig. 14). The FEFET potential profile for RESET and SET states at $V_G=0V$ (Fig. 15) show a larger channel potential and smaller source barrier for the SET state due to the P -switching in FE. Due to P -switching with smaller steps, a smaller change in V_T is observed in the I_D - V_{GS} characteristics (Fig. 16) at lower T_{FE} ($\sim 5nm$). Note that the V_T shift between $V_{SET}=3.4V$ and $3.6V$ is insignificant as P -switching takes away from the S/D side and thus has less impact on source barrier. Moreover, we observe an increased memory window ($MW=\Delta V_G$ at $I_D=1\mu A/\mu m$) (Fig. 17) for higher T_{FE} ($=10nm$) due to nucleation dominated P -switching. The MW decreases, and V_T shift becomes smaller for lower T_{FE} ($=5nm$) due to denser domain pattern and DW motion based P -switching, however, leads to multi-level memory operation.

I_D - V_{DS} characteristics for FEFET ($T_{FE}=5nm$) with SET state illustrates hysteretic characteristics (Fig. 18(a)) similar to experimental results in [11]. In the forward path, I_D increases with the increase in V_{DS} and exhibits a sharp decrease at some critical V_{DS} . This is because, the increase in V_{DS} leads to P -switching via domain wall motion near the drain side (Fig. 18(b)) due to negative V_{GD} . This results in an increase in drain-to-channel barrier which reduces I_D . In the reverse V_{DS} sweep, the reduced I_D state is retained due to P -retention and follows a different path from the forward sweep. The critical V_{DS} (which triggers P -switching) increases with the increasing T_{FE} (Fig. 19) and increasing V_{GS} (Fig. 19).

Note that, due to the 2D nature of our simulation, the MD state formation occurs only along the channel length. However, due to the polycrystalline nature of HZO, MD state can form along the width direction also. Consideration of MD state along the width can potentially lead to a gradual V_T shift, as well as a gradual V_{DS} induced decrease in I_D as shown in experiments [2,11].

V. NON-HYSTERETIC OPERATION WITH ENHANCED EFFECTIVE PERMITTIVITY (ϵ_r) OF GATE STACK

Let us now turn our attention to T_{FE} scaling below 5nm. The measured capacitance-voltage (C - V) characteristics of MFIS stack (Fig. 20(a)) with 2.5nm HZO/0.8nm SiO₂/p-Si as is shown in Fig. 20(b) suggesting a higher capacitance compared to a physically equivalent MOS capacitor (2.5nm HfO₂/0.8nm SiO₂/p-Si). This

suggests enhanced- ϵ_r behavior of HZO. The simulated C - V characteristics show good agreement with the experimental results (Fig. 20(b)). The P and E -field profile of FE-DE layer of the MFIS stack (Fig. 21) show that the FE layer is in the MD state with a dense domain pattern and no P -switching occurs within the operational voltage range (0-1V). Instead, the charge response is due to the background permittivity of FE and change in polarization magnitude ($|P|$) and not due to the change in P -direction through domain nucleation or DW motion. Enhanced- ϵ_r stems from the fact that some stray E -field lines between the domains with opposite P at 0V (Fig. 21(a)) transforms into out-of-plane component at -0.5V (Fig. 21(b)). To understand this phenomenon, a two dipole (with opposite dipole moment) model has been depicted in Fig. 22, where the dipoles are analogous to the domains with opposite P direction in FE. First, note that at 0V, there are stray E -fields lines between the dipoles (Fig. 22). Now, with the increase in voltage, $|P|$ in $+P$ domain increase and $-P$ domain decreases. That leads to a decrease in the stray E -field between the dipoles. Instead, an out-of-plane E -field by compensating more charges at the FE-DE interface. The additional charges on the FE interface from this transformation of stray E -field to out-of-plane E -field leads to an enhanced effective ϵ_r behavior of the FE layer. The simulated FEFET characteristics with 2nm HZO is shown in Fig. 23 showing an improved I_D and subthreshold swing (SS) compared to a FET with 2nm HfO₂. Note that the stray E -fields exist near the DW. As the domain and DW density increases with the decrease in T_{FE} , the stray E -field in the FE layer increases. Thus, stray E -field can be transformed into out-of-plane E -field to a larger extent leading to an increase in effective- ϵ_r of FE with the decrease in T_{FE} (Fig. 24). Therefore, the SS improvement in FEFET is more significant compared to HfO₂-FET with the decrease in oxide thickness (Fig. 25).

VI. CONCLUSION

In summary, we analyze the FEFET characteristics with $T_{FE}=5nm$ - $10nm$ for memory operation where the number of memory state can be increased in scaled FEFET by reducing the T_{FE} so that the DW motion becomes preferable P -switching mechanism over domain nucleation. In addition, we investigate the origin of enhanced- ϵ_r behavior of thin (1.5nm-3nm) FE layer as an outcome of electrostatic multi-domain interaction in dense MD state and analyze its influence in FEFET for logic operation. The trends obtained from our model for different T_{FE} in terms memory and improved-SS logic operation show good agreement with existing experimental FEFET results (Fig. 26).

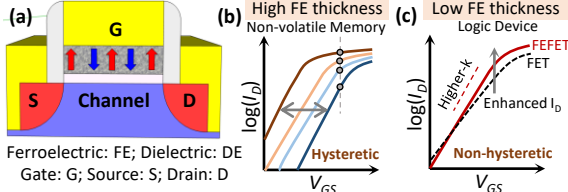
ACKNOWLEDGMENT

This work was supported by SRC under the contract no. 2020-LM-2959 and NSF under the grant no. 1814756.

REFERENCES

- [1] K. Chatterjee, et al., *IEEE Electron Dev. Lett.*, vol. 38, no. 10, 2017.
- [2] M. Jerry et al., *IEDM* 6.2.1-6.2.4, 2017.
- [3] D. Kwon et al., *IEEE Electron Dev. Lett.*, vol. 40, no. 6, 2019
- [4] D. Kwon et al., *IEEE Electron Dev. Lett.*, vol. 41, no. 1, 2020
- [5] S. Deng et al., *VLSI Tech.*, 2020.
- [6] A. K. Saha et al., *IEDM*, pp. 13.5. 1-13.5. 4 2017.
- [7] A. K. Saha et al., *DRC*, 2018.
- [8] K. Ni et al., *VLSI Tech.*, 2018.
- [9] H. W. Park et al., *Adv. Mater.*, vol. 31, no. 32, pp. 1805266, 2019.
- [10] A. K. Saha et al., *Scientific Reports*, vol. 10, no. 1, 2020.
- [11] M. Jerry et al., *DRC*, 2018.

FEFET Applications and Modeling Approaches



Previous work –

- [6] Uses 1D Landau-Khalatnikov equation. Assumes Homogenous P along FE thickness.
- [5] Area dependent number of domains. Number of domain does not depend on FE thickness (T_{FE}).
- [7,8] Captures multi-domain polarization as a macroscopic/average effect.

This work –

- Uses 2D Ginzburg-Landau equation. Captures P gradient along FE thickness.
- Electrostatic driven domain formation. Number of domain depends on T_{FE} .
- Captures Electrostatic driven domain nucleation and domain-wall motion
- Captures microscopic interaction of multi-domain polarization.

Fig. 2: Comparison of modeling approaches between previous work [5-8] and this work.

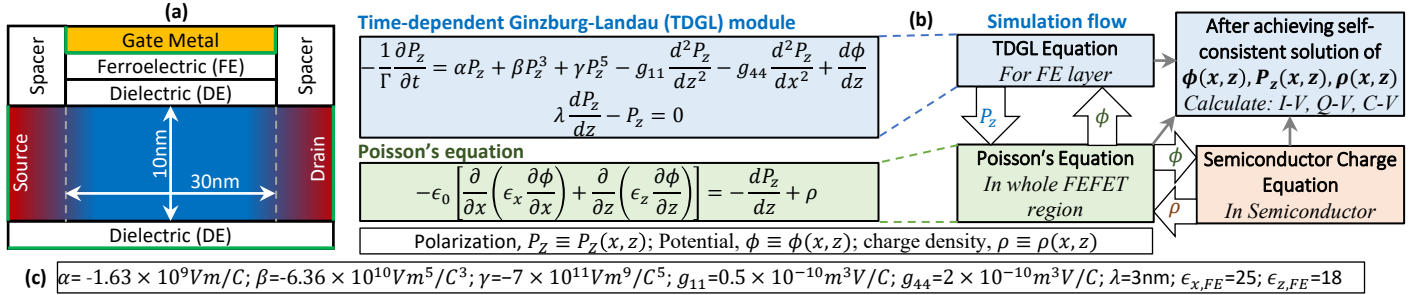


Fig. 3: (a) Simulated FeFET structure, (b) self-consistent simulation flow among TDGL, Poisson's and semiconductor (silicon) charge equations (c) FE parameters used in FEFET simulation. For the simulation of metal-FE-insulator-metal (MFIM) stack only Poisson's and TDGL equations are used.

Calibration and Validation of Phase-field Model and Multi-domain Polarization Switching in MFIM stack

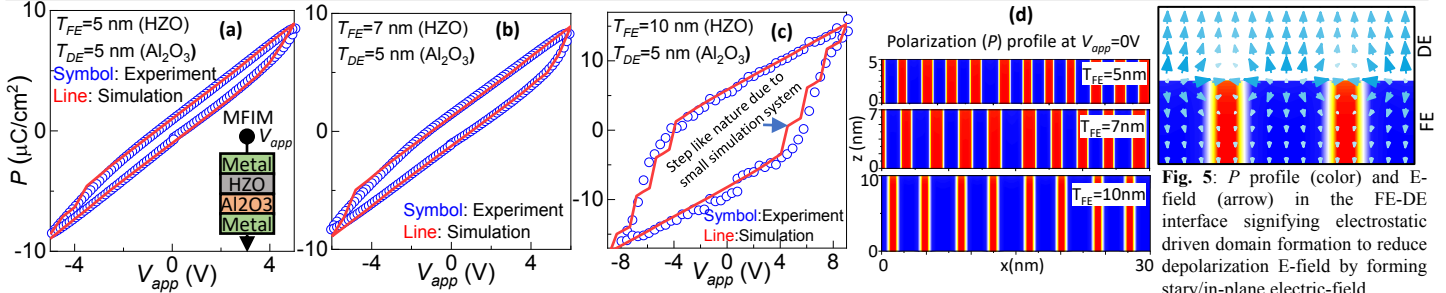


Fig. 4: (a) MFIM stack; (b-d) Experimental and Simulated P - V_{app} characteristics of MFIM stack for different FE thickness (T_{FE}); (e) P profile of FE in MFIM stack for T_{FE} at negative remanent state ($-P_R$). Red (blue) color corresponds to $+$ ($-$)P domains.

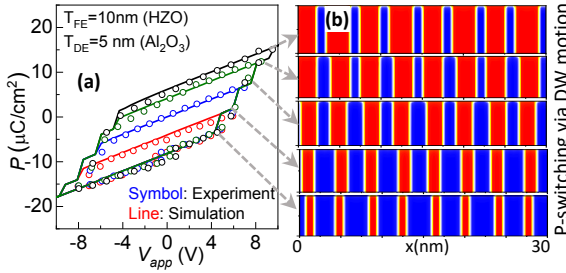
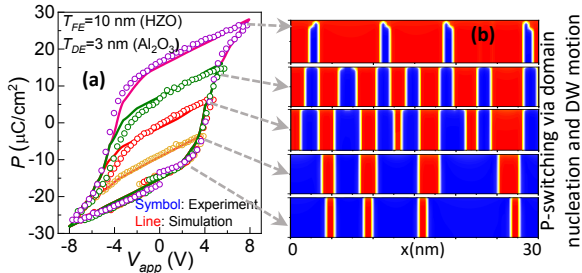


Fig. 6: (a) Partial P -switching characteristics in MFIM stack. (b) Corresponding P profile signifying domain nucleation and domain-wall (DW) motion based P -switching. $T_{FE} = 10 \text{nm}$, $T_{DE} = 3 \text{nm}$.

Fig. 7: (a) Partial P -switching characteristics in MFIM stack. (b) Corresponding P profile at different V_{app} signifying DW motion-based P -switching. $T_{FE} = 10 \text{nm}$, $T_{DE} = 5 \text{nm}$.

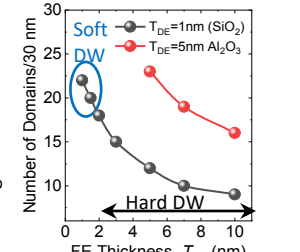


Fig. 8: Number of domains as a function of T_{FE} for different T_{DE} showing that the domain pattern becomes denser with decreasing T_{FE} .

FEFET characteristics with FE thickness (T_{FE}) of 10nm

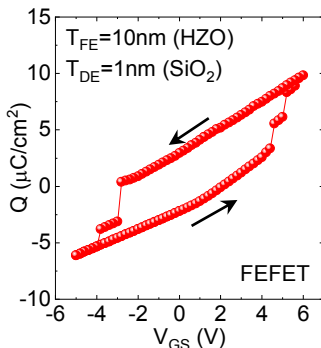


Fig. 9: Simulated gate charge (Q) vs V_{GS} at $V_{DS} = 0 \text{V}$ of FEFET showing hysteretic characteristics demonstrating the P -switching in the FE layer.

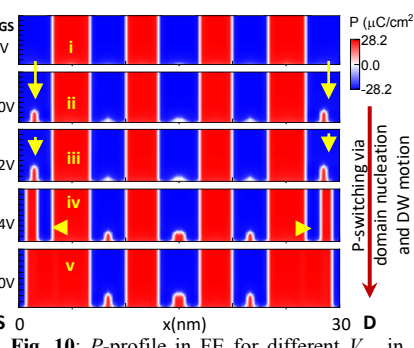


Fig. 10: P -profile in FE for different V_{GS} in FEFET showing domain nucleation (i-iv) followed by DW motion (iv-v) based P -switching. Note: P -switching is dominant near the source (S) and drain (D) region.

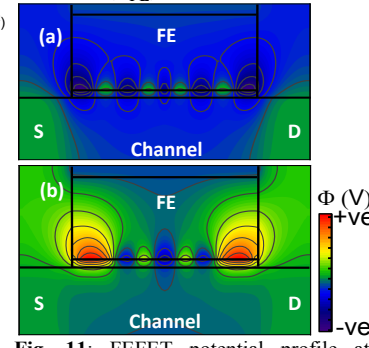


Fig. 11: FEFET potential profile at $V_{GS} = 0 \text{V}$ after (a) $V_{RESET} = V_{GS} = -5 \text{V}$ and (b) $V_{SET} = V_{GS} = 6 \text{V}$ showing P -switching induced change in channel potential as well as non-uniform potential in channel.

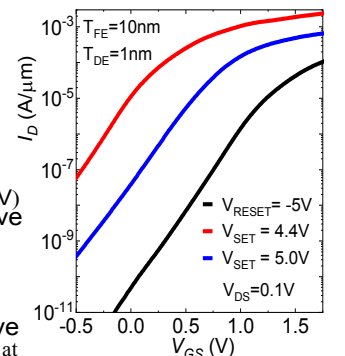


Fig. 12: (a) I_D - V_{GS} characteristics of FEFET for different V_{SET} showing the P -switching induced V_T shift and memory behavior.

FeFET Characteristics with FE thickness of 5nm

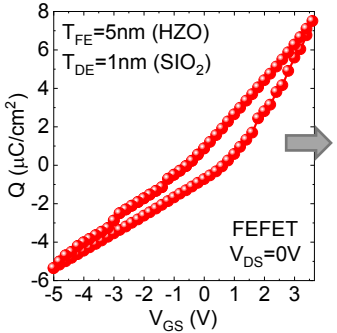


Fig. 13: Simulated $Q-V_{GS}$ of FEFET showing hysteretic characteristics for $T_{FE}=5\text{nm}$ due to DW motion.

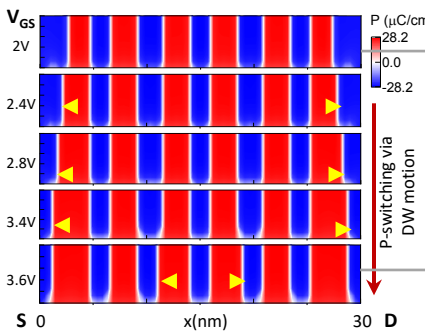


Fig. 14: P profile in FE for different V_{GS} in FEFET showing DW motion-based P-switching. Yellow arrow points towards the DW motion

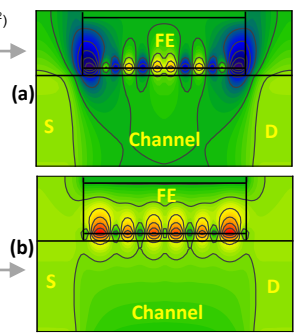


Fig. 15: FEFET Potential profile at $V_{GS}=0\text{V}$ after (a) $V_{RESET}=-3.6\text{V}$ and (b) $V_{SET}=3.6\text{V}$ showing P-switching induced change in channel potential.

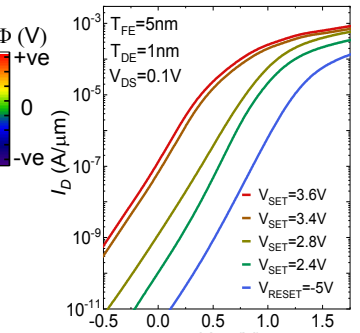


Fig. 16: (a) I_D-V_{GS} characteristics of FEFET with $T_{FE}=5\text{nm}$ showing multi-level memory operation.

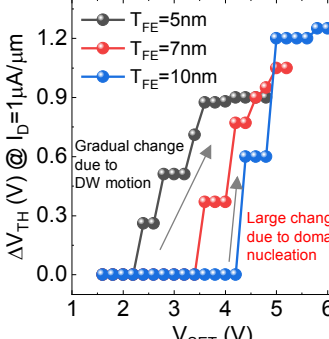


Fig. 17: (a) Memory window (ΔV_{TH}) for different T_{FE} and V_{SET} showing that MW increases with the increase in T_{FE} .

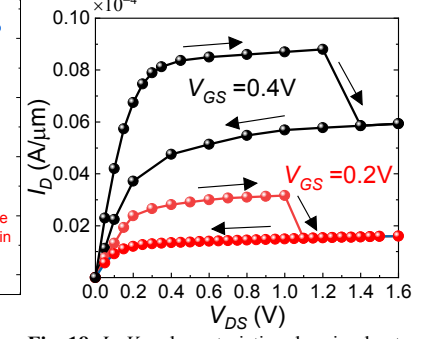


Fig. 18: I_D-V_{DS} characteristics showing hysteretic behavior. The P profile of the FE layer is shown for $V_{DS}=0.6\text{V}$ considering (b) forward sweep and (c) reverse V_{DS} sweep. Due to the P-switching near drain side the drain barrier height increases leading to a lower current in reverse sweep compared to forward sweep.

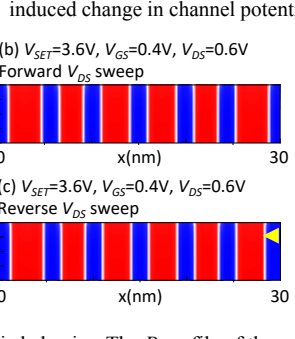


Fig. 19: V_{DS} to induce P-switching in drain-side for different V_{GS} showing P-switching occur at higher V_{DS} for increasing T_{FE} .

FeFET Characteristics with FE thickness from 3nm to 1.5nm (Low voltage operation → No P-switching)

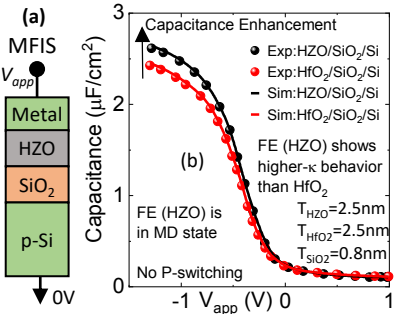


Fig. 20: (a) MFIS stack; (b) C-V characteristics of MFIS stack compared to MOS capacitor showing high-k behavior of the FE layer.

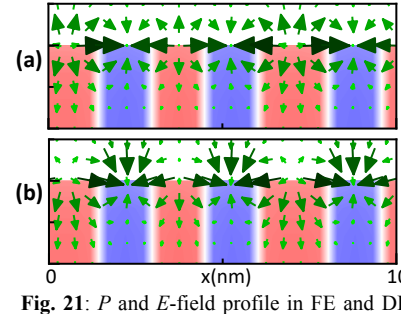


Fig. 21: P and E -field profile in FE and DE layer of the MFIS stack at (a) 0V and (b) -0.5V showing the transformation of stray in-plane E -field to out-of-plane E -field due to the magnitude change of P . This phenomena leads to extra charge in FE-DE interface leading to enhanced effective ϵ_r in FE layer.

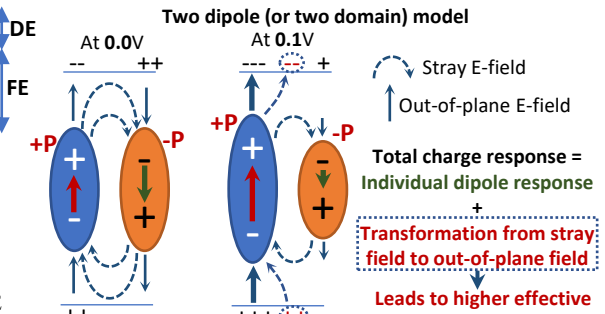


Fig. 22: Two dipole (or domain) scenario describing the origin of enhanced- ϵ_r of hard multi-domain thin FE film as a voltage induced change in dipole interaction associated electric field.

T_{FE}	Experimental Characteristics	Model Prediction
10nm	Hysteretic [Ref-2]	Hysteretic
5.5nm	Hysteretic [Ref-1]	Hysteretic
2.8nm	SS improvement [Ref-4]	SS improvement
1.8nm	SS improvement [Ref-3]	SS improvement

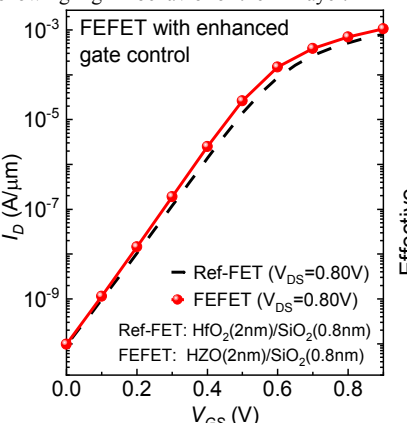


Fig. 23: (a) I_D-V_{GS} characteristics of FEFET showing higher-k behavior with enhanced gate control compared to Ref-FET (with $\text{HfO}_2/\text{SiO}_2$ gate stack).

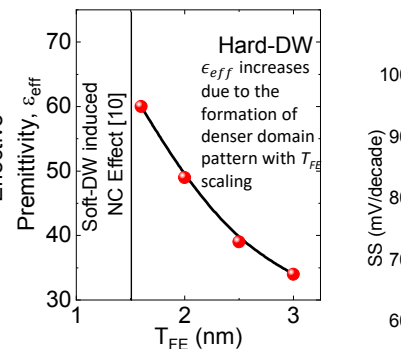


Fig. 24: Effective permittivity of the FE layer for different T_{FE} showing that permittivity increase with the decrease in FE thickness.

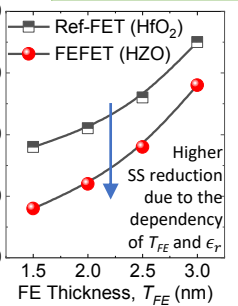


Fig. 25: Subthreshold swing (SS) for different $T_{FE}=T_{\text{HfO}_2}$ showing more SS reduction in FEFET.

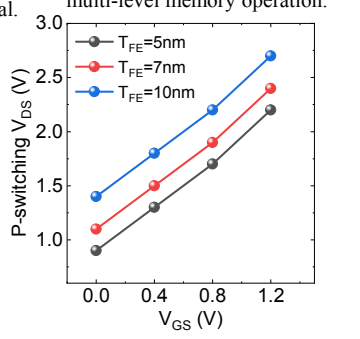


Fig. 26: (a) T_{FE} dependent experimental characteristics of FEFET in different earlier works. (b) Co-relation between T_{FE} and FEFET characteristics and its application.